Journal of Thermal Analysis and Calorimetry
https://doi.org/10.1007/s10973-022-11848-w

Raw kaolinitic–illitic clays as high-mechanical-performance hydraulically pressed refractories

Milica Vidak Vasić[1] · Lidija Radovanović[2] · Lato Pezo[3] · Zagorka Radojević[1]

Received: 2 March 2022 / Accepted: 27 November 2022

Abstract

The usage possibility of 19 composites of raw refractory clays from Serbia containing approximately 53.29% of SiO_2 and 26.73% of Al_2O_3 is presented. The sum of fluxing oxides was 57.74%, while these materials contained 32% of quartz, 29% of kaolinite and 26% of illite–mica. Dilatometry tests revealed a sudden shrinkage with the peak at approximately 1115 °C, owing to the formation of mullite. The refractoriness was in the range of 1581–1718 °C, which classifies the composites from low- to high-duty refractories. Based on correlation analysis, the refractoriness mostly depended on the content of alumina. The lightness of the fired test pieces was lower after firing when compared to the dry samples, and it decreased with the firing temperature from reddish to grayish. The study presents a novel attempt to define all the necessary properties of raw refractory clays and products fired at the 1100–1300 °C range on a laboratory level. Most of these clays can be used as natural refractory materials for ceramic and glass furnace lining. The organic matter in some of the samples influences negatively the fast-firing process.

Graphical Abstract

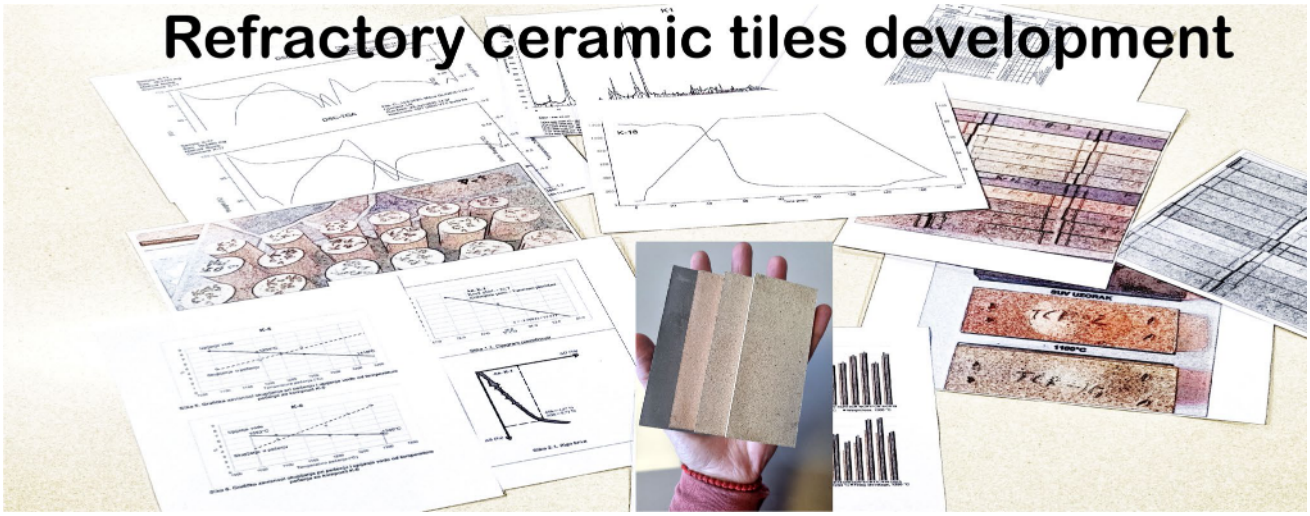

Keywords Raw kaolinitic–illitic clays · Refractories · Water absorption · Sintering range · *L*a*b** color space

Introduction

The term "refractory clays" implies materials that can withstand service temperatures above 1100 °C, but preferably higher than 1500 °C [1]. These materials contain

✉ Milica Vidak Vasić
milica.vasic@institutims.rs

Extended author information available on the last page of the article

Published online: 24 December 2022

relatively low amounts of fluxes (SiO_2, Fe_2O_3, Na_2O and K_2O) and can be used in the linings of industrial ovens, furnaces, kilns, reactors, etc. Among other minerals, kaolinite is the most desirable component in refractory clays as the source of alumina. Kaolinitic clays show several more advantages in these terms, like fine particle size, chemical stability, good mechanical characteristics and pale firing color. The illitic component in the clays decreases refractoriness, while quartz shows adverse effects depending on its quantity and particle sizes, and finally the applied firing temperature [2].

Clay deposits in Serbia are predominantly of illite–mica type, with a dominant quartz content, sometimes significant feldspar and carbonate quantities, and minor amounts of kaolinite, chlorites, smectites and hematite [3, 4]. The deposit in Serbia examined in this study is a relatively rare example of raw clays containing increased content of clay minerals, which were expected to be suitable in the production of refractory materials. Considering that the products for the construction of furnace ceilings are mainly imported by the Serbian industry, it is necessary to further study the available domestic deposits. The proper utilization of natural resources in Serbia demands deeper scientific and technological research. The need to replace the walls of the furnace and the wagon refractory materials largely depends on the equipment of the factory and the attitude of the management. If the tunnel kiln is often stopped, there is an increased necessity to replace the ceilings. Also, as far as wagons are concerned, depending on the handling when removing final products, there can be a frequent need to replace refractory parts. Unreplaced truncated parts of the wagon bring further problems in the production process, such as "false" environmental air [4].

Refractory materials are a special group of minerals of diverse nature and application possibilities. Some examples of refractories are porcelain, electro-porcelain, chamotte, steatite, calcium silicate bricks [5], etc. With heterogeneous, natural materials, it is very difficult to follow all the reactions that take place during firing and find the appropriate application, and this part is insufficiently presented in the literature. Therefore, this paper deals with the assessment of the quality and possibilities of the application of natural refractory clays.

This study is the first known attempt to summarize all the necessary information on a newly opened raw refractory deposit and find its optimal applications. To determine the optimal mixture of raw materials, it is essential to learn the ceramic and technological behavior of materials at different firing temperatures and to relate them to important properties of the initial material like chemical and mineralogical composition, thermal behavior and refractoriness. Additionally, the first colorimetric evolution of refractory clays gave important details on mineralogical composition after firing. Besides, the interesting relations between the fired color and ceramic behavior of the samples are noticed.

Materials and methods

Clay deposit in Crne Rovine is located in the freshwater sediments of eastern Serbia, stratigraphically belonging to the lower Jura. In a lithological sense, the sediments consist of clay and sandstone. Charcoal clays with rare limestone interlayers are less often present. All of the above members vary in mineral composition, color, diagenesis degree and depth of the partitions and intercalations. Sandstone and sandy clays are found under the humus blanket. The sandstones are large, poorly tied and yellow to yellowish red, while the clay is yellow to dark. Beneath sandstone and sandy clay, there is a productive layer of refractory clays of different hues of gray. The selected deposit is anticipated to provide 100,000 t of raw material a year, which represents an excellent opportunity to considerably lower the importation of such refractories in Serbia.

The 19 composites of raw clays from Serbia were tested before the exploitation phase. The composites were formed as mixtures of 132 partial samples (0.5–42.60 m in depth) from 11 drill holes. The composites of interest contained the parts or whole drill holes and are labeled CR1–CR19. Firstly, partial trials are done in the laboratory to determine the most important characteristics like chemical composition, shrinkage, water absorption, etc. Then, the composites were designed to contain equal quantities relative to the depth of sampling and position of the drill holes which is convenient in terms of future extraction. Several partial trials were excluded from the mixes due to relatively high contents of carbonates (8.40%), high content of Fe_2O_3 (up to 7.94%) and low quantity of Al_2O_3 (below 22%), and also bloating of samples at higher temperatures (1250 °C).

The raw samples were mixed to produce the previously defined composites, dried in an oven at 105 °C to the constant mass and afterward tested to determine particle size distribution. The composites were sieved through a set of standard sieves. The remains on each sieve were measured with an accuracy of 0.01 g. Fractions below 0.063 mm were tested by the hydrometric method, while the solution of sodium hexametaphosphate was used as a dispersing agent (anticoagulant) of the fine-grained particles [6]. The particle size fractions were clay (< 0.002 mm), silt (0.002–0.06 mm) and sand (0.06–2 mm).

Further preparation of the composites included graining in a mill using tungsten carbide balls (Herzog HSM 100H, Germany). The fractions below 0.5 mm were accepted for further tests and forming of the samples. Besides, the remains on a 0.063 mm sieve were determined by the wet

method and later observed by using a polarizing microscope by Ernst Leitz, Germany [7].

The chemical and mineralogical composition of the composites is determined using the same methodology and equipment reported previously [7]. The energy-dispersive X-ray fluorescence (XRF) technique was employed to determine the chemical composition. The used instrument was Spectro Xepos, with a 50 W/60 kV X-ray tube. The calibration of the instrument is done by using certified reference materials NCS DC 60102 and the set of the ten reference materials (from JRRM 302 to JRRM 310). The certified reference materials were used for validation of the method as well (NCS DC 60104, NCS DC 60105 and NCS DC 60106). The range of error for these materials was ± 0.62%. X-ray diffraction analysis (XRD) was carried out using the Philips 1050 X-ray powder diffractometer operating with Ni-filtered Cu$K\alpha$ radiation ($\lambda = 1.5418$ nm) and Bragg–Brentano focusing geometry. The patterns were taken in the 6–70° 2θ range with the step of 0.05° with an exposure time of 6 s per step. The identification of the minerals was based on the Inorganic Crystal Structure Database (PDF-2). The diffractograms were treated by EVA v.9v0 software package and the reference intensity ratio (RIR) method [8] to determine semiquantitative phase analyses. The mineralogical composition of raw and selected fired samples is performed.

The thermal behavior of the composites was investigated by simultaneous differential thermal analysis and thermogravimetry (DTA/TGA) on an SDT Q600 (TA instruments) device up to 1000 °C in an air atmosphere using platinum sample cups. The mass of the samples varied from about 15–20 mg. The flow rate was 100 mL min^{-1}, while the heating rate was 20 °C min^{-1}. Dilatometry tests are done in the air atmosphere with a flow of 20 mL min^{-1} (Setaram instrumentation). The heating speed was 20 °C min^{-1}, and the retention time at 1200 °C was 1 h. The calibration curve was recorded in the same conditions.

Refractoriness was determined as the temperature of the commencement of softening of materials by using equivalent cones and cones made from the sample tested [9, 10]. Standard-defined firing regime conditions [10] are 15 °C min^{-1} up to 200 °C and 2.5 °C min^{-1} during further heating. Since the estimated refractoriness of the tested samples is higher than 900 °C, the following regime has been applied: 15 °C min^{-1} up to 900 °C and 2.5 °C min^{-1} until the end of the test. The test procedure is almost identical to ASTM standard [11], the temperatures of refractory deformations are the same, while there is a difference from the German scale of incandescent gauges (Seger cones—SC).

The dry masses after milling were used to determine the remaining on the 0.063 mm sieve (RS) and the quantity of total Mg and Ca carbonates (CCC) by Scheibler's volumetric method [12].

The dry composites were moistened by adding 4% of water and left to homogenize for 24 h. Later on, the moist material is sieved again through 0.5 mm sieves and then hydraulically pressed to form $120 \times 25 \times 8$ mm^3 tiles, by the same methodology as previously reported [7]. Besides, manually formed samples in the form of a cylinder of 30 mm in diameter and 40 mm in height were formed with 21.10% moisture on average. These samples were used to determine compressive strength. The plastic masses were also tested to discover the sensitivity to drying by Bigot [13] and the plasticity coefficient following Pfefferkorn's methodology [14]. After performing these tests, the test samples were dried gradually in an electrical laboratory oven until the constant mass is achieved.

The firing was conducted in an oxidizing environment laboratory electric furnace at 1100, 1200, 1250 and 1300 °C, with 1 h retention at the final temperature and natural cooling in a closed furnace. The used firing regime was 70 °C h^{-1} until 200 °C, then 92 °C h^{-1} up to 520 °C, 60 °C h^{-1} until 610 °C and finally 140 °C h^{-1} until reaching the peak temperature [7].

Water absorption (WA) was determined in the usual way, following standards for refractory bricks [15] and ceramic tiles [16], which propose a similar methodology. Water absorption under vacuum is performed using the apparatus Isovacum A 2012 by Gabtech, Italy. The three-point modulus of rupture was measured at ambient temperature by using Crometro CR4/E1 Gabrielli machine (Italy) of 1 N resolution, with a range of up to 7 kN, and 1 N s^{-1} of force increase. The bottom supports distance was 100 mm. All of the measurements of mass and dimensions were taken on a calibrated scale and caliper with the second decimal place precisions. The determined characteristics are frequently employed in the assessment and comparison of refractory product quality.

The surface micromorphology of the undisturbed surface of the chosen fired samples is studied using a Tescan MIRA 3 XMU field emission scanning electron microscopy (FE-SEM). Samples were coated with Au–Pd in a Fisons instruments chamber before the analysis.

The color of the raw composite samples and those pressed and fired in the 1100–1300 °C range was determined by using a portable spectrophotometer ColorLite (model SPH870). The high-powered LED light source and high-resolution technology enable a spectral scan in 3.5 nm steps in 0.5 s. Certified white standard PTB (Physikalisch-Technische Bundesanstalt) is used as a reference. The coordinates in color space were based on lightness (L^*), saturation (a^*) and intensity (b^*) [17]. The value of L^* that equals 0 corresponds to black, while 100 represents the white color. The other two coordinates are chromatic, $a^* > 0$ is associated with red, and $a^* < 0$ is with

green color. Positive values of b^* stand for yellow, while negative is for blue.

Pearson's correlation analysis was done for all the obtained parameters in this research to reveal the causal relationships between the initial composites and final products. The program used in the analyses was Statistica 10.0.

Results and discussion

Important properties of the composite materials

The chemical composition (Table 1) classified the examined composites into silico-aluminous and semi-acidic refractories [18, 19]. Additionally, the examined composites can be ranked as low-alumina fireclay [20].

Statistically significant correlations between loss on ignition (*LOI*) and Al_2O_3 (positive), and also *LOI* and SiO_2, Na_2O, K_2O and TiO_2 (negative) implied it mostly originated from clay minerals (Table 6 in Appendix). The relatively low content of TiO_2 was not influential in the development of the glassy phase [21]. The mass ratio between Al_2O_3 and Fe_2O_3 contents, being in the 7.83–20.05 range, classified the composites as rich in aluminum and suitable for the production of refractories [22]. The SiO_2/Al_2O_3 mass ratio in the 1.72–2.32 range would imply the pale/whitish fired color in the case of high-grade kaolin [22]. Being aware that Fe^{3+} and Ti^{4+} strongly influence the final product color since titania can enter the kaolinite structure by cation exchange and intensify the coloring impact of iron [23], this criterion is not applicable in the tested materials. Depending on the content of Fe_2O_3 the fired color of the composites was expected to vary between dark, red and white. With the content of Fe_2O_3 mainly below 3%, most of the composites belong to light-firing clays [24]. Besides, the sum of Fe- and Ti-bearing compounds below 6% in all the composites allows a beneficiation process application for obtaining the white products [25]. The studied composites contained the sum of Na_2O, K_2O, MgO and CaO in the range of 2.41–4.46%, which again classifies them as refractory materials [26]. Since a certain share of fluxing agents is usually added to kaolin that will have refractory properties [22], these composites are of valuable economical composition.

Mineralogical analyses revealed the composites were mainly kaolinitic–illitic, with the presence of quartz and minor amounts of hematite, calcite and zeolites (Table 2). Only a few of the samples were illitic–kaolinitic (CR1, CR2, CR8 and CR9). Iron was in the form of zeolites and

Table 1 Chemical composition of the composites

	LOI/%	SiO_2/%	Al_2O_3/%	Fe_2O_3/%	K_2O/%	MgO/%	CaO/%	Na_2O/%	SO_3/%	P_2O_5/%	MnO/%	TiO_2/%
CR1	13.12	51.89	26.04	3.33	1.51	1.17	0.86	0.36	0.18	0.14	0.02	0.90
CR2	11.23	54.49	26.35	2.52	1.58	0.97	0.83	0.57	0.22	0.06	0.01	0.88
CR3	14.57	51.70	27.30	2.66	0.57	0.57	0.82	0.32	0.07	0.07	0.01	0.98
CR4	15.08	50.13	27.77	2.68	0.79	0.80	0.68	0.44	0.12	0.08	0.01	0.95
CR5	14.87	50.48	27.56	2.44	0.68	1.01	0.67	0.42	0.31	0.07	0.01	0.99
CR6	13.34	52.37	27.55	2.83	0.81	0.71	0.55	0.36	0.05	0.06	0.03	0.94
CR7	16.21	48.85	28.10	2.72	0.90	0.90	0.53	0.40	0.20	0.08	0.01	0.83
CR8	11.64	54.98	26.57	2.75	1.31	0.64	0.62	0.36	0.05	0.08	0.01	1.01
CR9	9.44	57.21	24.70	3.08	2.49	0.84	0.45	0.54	0.10	0.05	0.03	0.96
CR10	11.92	55.05	25.62	3.03	1.40	0.87	0.39	0.35	0.03	0.06	0.02	1.02
CR11	10.15	56.85	25.70	2.47	1.55	0.91	0.44	0.56	0.07	0.07	0.02	1.21
CR12	11.25	54.59	25.87	2.35	2.52	1.11	0.36	0.47	0.08	0.06	0.02	0.99
CR13	10.97	56.20	25.48	2.39	1.95	1.00	0.38	0.51	0.04	0.06	0.01	0.96
CR14	11.37	54.42	26.24	2.46	2.37	0.86	0.44	0.41	0.03	0.07	0.03	0.91
CR15	11.69	54.23	26.08	3.07	1.77	0.88	0.42	0.49	0.04	0.06	0.04	0.92
CR16	13.65	52.03	27.85	1.98	1.19	0.95	0.47	0.34	0.04	0.07	0.01	0.92
CR17	14.89	50.20	29.18	1.46	1.55	0.68	0.23	0.43	0.03	0.08	0.03	0.88
CR18	11.04	54.52	27.46	2.01	1.77	0.82	0.48	0.36	0.08	0.06	0.01	0.98
CR19	14.47	52.41	26.54	2.62	0.95	0.67	0.69	0.34	0.03	0.07	0.01	0.95
Min.*	9.44	48.85	24.70	1.46	0.23	0.57	0.32	0.57	0.03	0.05	0.01	0.83
Max	16.21	57.21	29.18	3.33	0.86	1.17	0.57	2.52	0.31	0.14	0.04	1.21
Aver	12.68	53.29	26.73	2.57	0.54	0.86	0.42	1.46	0.09	0.07	0.02	0.96
SD	1.93	2.40	1.12	0.44	0.18	0.16	0.08	0.60	0.08	0.02	0.01	0.08

**LOI* Loss on ignition, *Min.* minimum, *Max.* maximum, *Aver.* average, *SD* standard deviation

Table 2 Semiquantitative phase analysis of the composites

	Quartz/%	Kaolinite/%	Illite–mica/%	Hematite/%	Anatase/%	Mutinaite/%	Faujasite/%	Magnesian calcite/%	Hydrotalcite/%	Total clay minerals content/%
CR1	28.00	31.20	33.40	1.00	2.20	2.20	0.40	1.60	0.00	64.60
CR2	33.30	24.70	33.70	0.50	2.20	3.50	0.30	1.80	0.00	58.40
CR3	29.60	44.00	23.10	0.50	1.90	0.00	0.00	0.90	0.00	67.10
CR4	30.50	37.50	24.00	0.80	2.30	3.90	0.00	1.00	0.00	61.50
CR5	33.10	31.30	26.50	0.90	2.10	5.20	0.00	0.90	0.00	57.80
CR6	27.10	39.80	27.40	0.70	2.70	1.00	0.00	1.30	0.00	67.20
CR7	20.50	43.80	26.60	1.00	2.30	4.80	0.00	1.00	0.00	70.40
CR8	45.80	23.10	27.50	1.00	1.70	0.90	0.00	0.00	0.00	50.60
CR9	40.10	24.40	27.30	0.80	2.00	5.40	0.00	0.00	0.00	51.70
CR10	37.50	32.40	25.20	0.90	1.70	2.30	0.00	0.00	0.00	57.60
CR11	37.10	32.00	25.90	0.80	1.90	2.30	0.00	0.00	0.00	57.90
CR12	28.10	33.40	28.50	0.60	1.70	3.30	0.00	0.00	4.40	61.90
CR13	34.00	31.90	27.30	0.80	1.70	4.30	0.00	0.00	0.00	59.20
CR14	33.60	32.00	27.40	0.60	1.50	4.90	0.00	0.00	0.00	59.40
CR15	36.10	34.50	22.10	0.70	1.30	5.30	0.00	0.00	0.00	56.60
CR16	33.30	37.40	21.90	0.90	2.20	4.30	0.00	0.00	0.00	59.30
CR17	21.30	45.80	22.40	0.60	2.70	7.20	0.00	0.00	0.00	68.20
CR18	28.80	42.90	23.20	0.40	2.10	2.60	0.00	0.00	0.00	66.10
CR19	37.10	36.90	18.40	0.40	2.00	4.40	0.20	0.60	0.00	55.30
Min.*	20.50	23.10	18.40	0.40	1.30	0.00	0.00	0.00	0.00	50.60
Max	45.80	45.80	33.70	1.00	2.70	7.20	0.40	1.80	4.40	70.40
Aver	32.36	34.68	25.88	0.73	2.01	3.57	0.05	0.48	0.23	60.57
St. Dev	6.16	6.67	3.76	0.20	0.37	1.82	0.12	0.63	1.01	5.51

*Min. – minimum, Max. – maximum, Aver. – average, St. Dev. – standard deviation

Table 3 Particle size distribution and contents of carbonates

	Minimum	Maximum	Average	SD
Clay fraction/% (< 0.002 mm)	10.84	52.00	27.15	11.70
Silt fraction/% (0.002–0.06 mm)	7.20	63.00	46.91	14.81
Sand fraction/% (0.06–2.00 mm)	3.00	56.00	22.05	14.57
Remains on the 0.063 mm sieve/%	1.80	41.56	21.06	12.49
Total contents of carbonates/%	0.00	1.60	0.21	0.45

**SD* Standard deviation

hematite. Since the highest content of kaolinite, the sample CR17 presumably can present the most appropriate material for the refractory application. Additionally, the CR17 contained the lowest quantity of quartz. The correlation analysis proved that the increased content of kaolinite meant a decreased quantity of quartz and illite–mica (Table 7 in Appendix).

According to the granulometric composition before milling, the composites belonged to different types concerning soil texture diagrams. All of the contents of fractions varied greatly. On average, the silt fraction predominated in the composites (Table 3). After milling, the remains on the 0.063 mm sieve were also determined. These remains were monitored by using a polarizing microscope and seen as composed of gray and yellowish clay leaf grains, fragments of gray color and slatelike texture, yellowish brown aggregates most likely of clay–silicon composition, quartz and parts of a limestone.

The content of carbonates in all the composites is considered low and met the requirements of the standard for CaO content below 1.00% [27] for materials of potentially high refractory properties.

Thermal analyses of the composite materials

DTA/TG analysis

All of the DTA curves (Fig. 1) were similar in shape to the two pronounced endothermic peaks. The first endothermic peak in the range of 60 to 75 °C is related to the loss of interlayer water in illite–mica and minor adsorbed water in kaolinite [29]. The second peak (495–515 °C) is owed to the removal of hydroxyl moisture of illite–mica and kaolinite [28, 29] while forming metakaolin and meta-illite, but also some amorphous matter. A mild endothermic peak in the interval of 352–500 °C indicates the presence of alumina hydroxide [28] and is most pronounced in CR1 and CR3. This peak is overlapped by an exothermic reaction that accompanies the decomposition of organic matter in about 300–500 °C range. The peaks maxima corresponding to organic matter oxidation were mostly noticed at about 400 °C. According to the relative intensity of these peaks, it appeared that the composites containing the highest quantity of organic matter were CR16 and CR5, respectively. A quartz polymorph transition peak at about 571 °C is rarely distinguished in DTA diagrams of these samples since it is superimposed on dehydroxylation [29, 30]. The absence of characteristic endothermic peaks at about 670–700 °C indicates that montmorillonite was not present in the composites [28], which is confirmed by the XRD analysis. Sample CR2 is characterized by two mild peaks which continue on top of each other at about 777 and 850 °C. These peaks consequently present the decarbonization of small amounts of calcite and magnesite [12]. Smaller endothermic peaks in all samples in the 934–971 °C interval indicate a violation

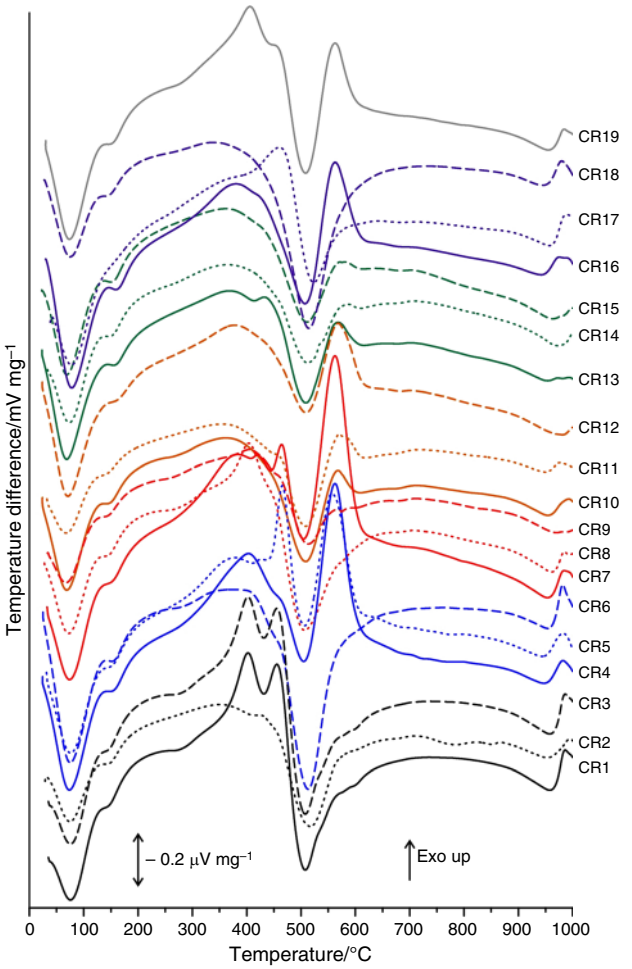

Fig. 1 DTA analysis of the studied composites

of the crystal lattice of illite–mica [28]. The exothermic peaks at 946–990 °C correspond to the crystallization of Al-Si spinel, primary mullite ($2Al_2O_3{\cdot}SiO_2$) and amorphous silica [29, 31]. These peaks are evident in all the composites except the CR9, CR12, CR14 and CR15, in which they probably would have appeared at temperatures above 1200 °C [22, 26].

To determine the thermal stability of the composites, the TG analysis was performed in an air atmosphere and the results are presented in Fig. 2. Thermal decomposition of all composites happens in four overlapped steps which correspond to the four peaks at DTA curves (Fig. 1).

The intensive mass loss is seen at the beginning of firing (up to about 200 °C), which is related to the loss of interlayer water in illite–mica and adsorbed water molecules in kaolinite [29]. In the period of up to 200 °C, the highest mass loss is observed in the decreasing order in CR6, CR1/CR17 and CR3/CR4, mainly due to the highest total contents of total clay minerals (Table 2) [12]. The most intensive mass loss was recorded between 400 and 600 °C, when dehydroxylation of the clay minerals, the most intensive part of the organic matter combustion and phase transition of quartz occurred. The later period appeared as the most pronounced in the corresponding differential TG (DTG) diagrams, while the peaks appeared at the same temperature as the endothermic peak of clay minerals dehydroxylation, showing the magnitude of the impact. In between these periods, constant and slow mass loss appeared [12]. In the range of 200–600 °C, the most emphasized mass loss is observed in CR7, due to the highest content of both organic matter and total clay minerals. CR2 experienced atypical behavior in the studied group of 19 composites in a period of 718–869 °C. This period is characterized by a constant mass loss owed to a small share of carbonates. The peaks are distinguished in DTG curves to maximum loss at about 781 °C (calcite decomposition) and 850 °C (magnesite) [12]. CR1 also contained some dolomite (Tables 1 and 2),

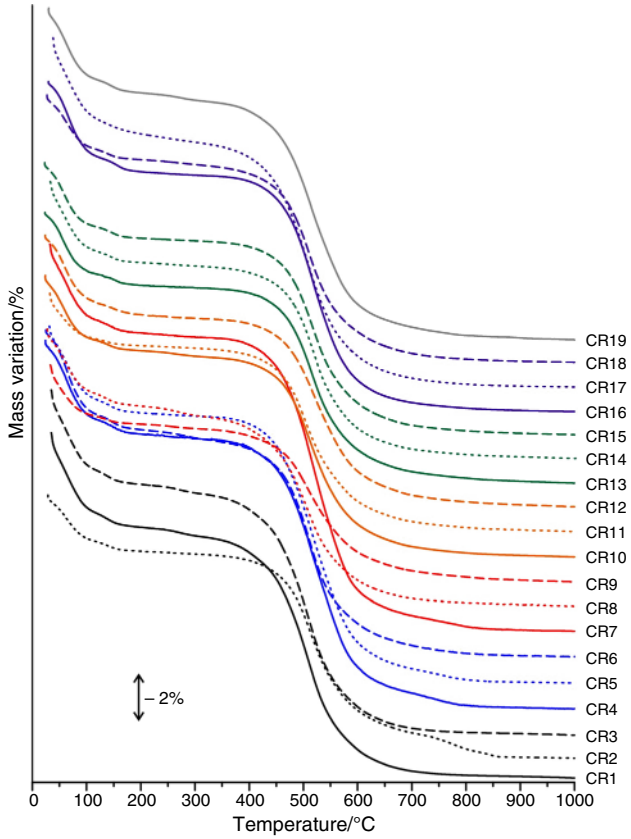

Fig. 2 TGA analysis of the studied composites

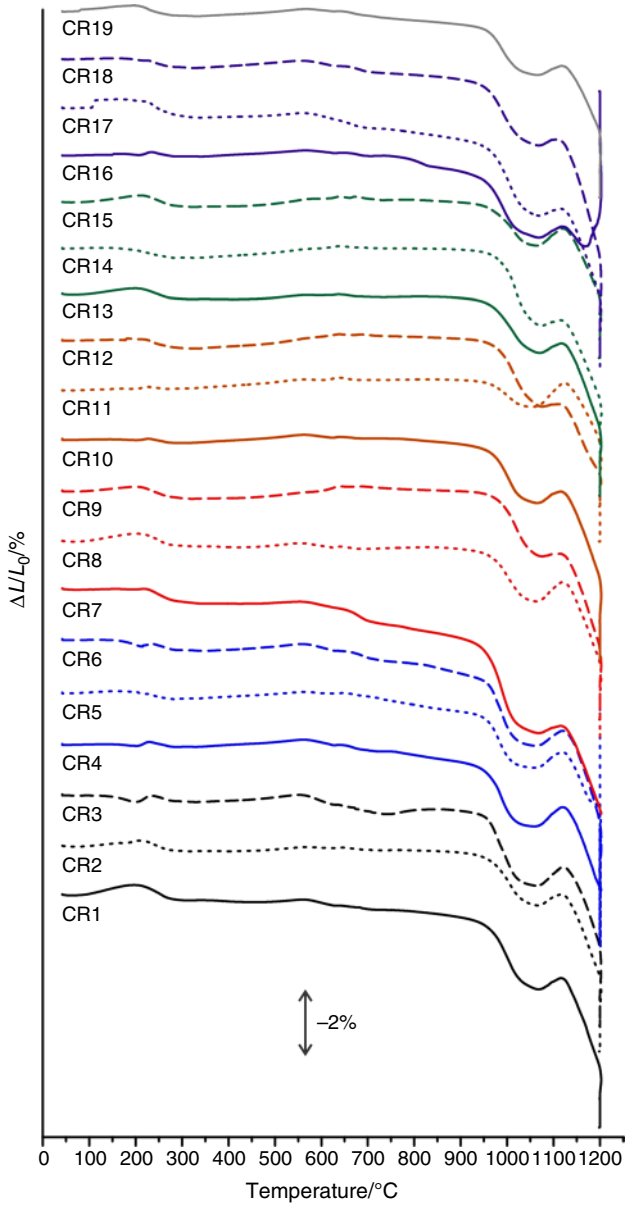

Fig. 3 Dilatometry analysis of the studied composites

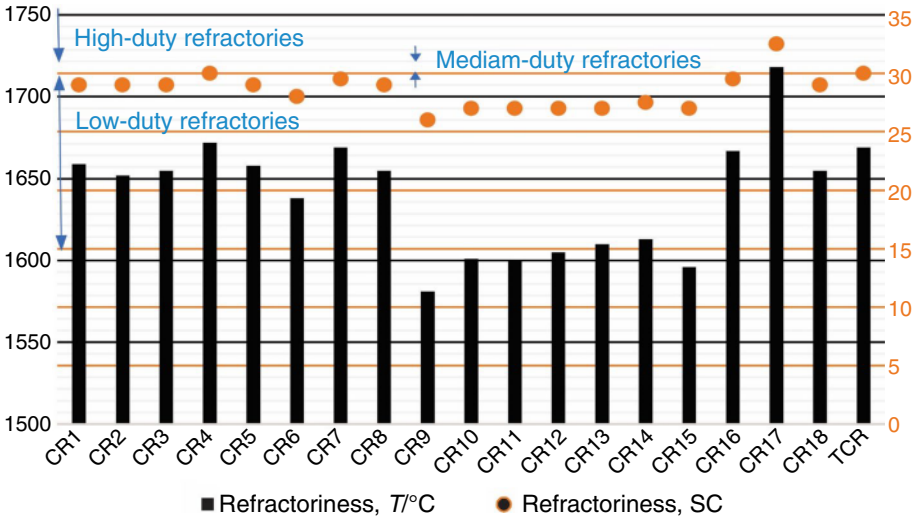

Fig. 4 Relationships between refractoriness temperature and Seger cones (SC) to service possibilities of the tested composites (15 < SC < 29 low-duty, 29 < SC < 31.5 medium-duty, 31.5 < SC < 33 high-duty refractories)

this effect in the thermal analysis was less pronounced and visible only in DTG curves. In the continuation of firing from 600 °C onwards, all the composites additionally lost between 1.1 and 1.9% of the mass. According to the TGA curves, the total mass loss of composites is in the range of 9.26–16.53%. The smallest mass loss was found for CR9, while the biggest is observed for CR7, which can be associated with the contents of clay minerals.

Dilatometry

The behavior of composites during the firing process up to 1200 °C (Fig. 3) was followed by dilatometry analysis to supplement the results of the corresponding DTA and TGA curves. The tested samples exhibited dilatometric curves of mutually similar shapes, with the CR5 and CR16 as an exception. In the period of up to 200 °C, negligible dimensional changes occurred. Some composites experienced a mild expansion (up to 0.3%), while others slightly shrank (up to 0.2%). Further, a period of slow shrinkage, in some cases including periods of mild spreading, lasted up to 964 °C (CR10) and amounted to up to 1.74% (CR7). This shrinkage is mostly due to the transformation of clay minerals into metakaolin and meta-illite [32]. Viscous flow sintering that causes the intensive formation of amorphous phase and structure reorganization [24] initiated in these composites in the 919 °C (CR1) – 964 °C (CR10) range, which is accompanied by a sharp shrinkage. The most intensive contraction in this period occurred in the composite containing the highest quantity of total kaolinite and illite–mica, which was the CR7. Besides, the decreased quantity of quartz influenced a decrease in shrinkage in this period [22]. In some cases, a low-extent expansion is seen at about 575 °C due to quartz presence (CR1, CR3, CR4 and CR6). Within the temperature region of 200–900 °C, the CR12 and CR14 experienced the lowest shrinkage (of about 0.08%). These samples contained the average content of clay minerals in the studied group, while the most significant difference was in the highest content of silt fraction. The CR11 was the only sample that experienced some expansion in this period, which amounted to 0.17%. Some of the composites experienced slightly faster shrinkage at temperatures above 700 °C. The effect was most pronounced in the CR16 and began at about 744 °C. That is probably caused by the high quantity of kaolinite and among the lowest contents of illite [33]. The mild shrinkage was followed by an intense collection which marked the commencement of sintering and the complete separation of crystalline water and degradation of the crystal lattice of clay minerals. This is the moment when metakaolin and meta-illite start to transform into spinel-like phases and amorphous silica, accompanied by the separation of fluxing oxides, which is seen as shrinkage of the material [34].

The first period of intensive shrinkage in composites is finished between 1050 (CR11) and 1076 °C (CR12) when the peaks are reached due to the completion of the primary mullite formation [28, 35]. The additional shrinkage up to the sintering temperature was in the range of 0.73 (CR11) and 2.65% (CR7). The higher content of quartz induced an increased shrinkage in this period, as per correlation analysis (results not shown).

Above 1100 °C, samples showed expansion from 0.07 (CR12) to 0.72% (CR11) with peaks at around 1105 (CR12) and 1125 °C (CR3), due to the crystallization of cristobalite [28, 36, 37]. The dilatation at high temperatures can also be influenced by the content of fluxes, especially alkali oxides [38].

The final shrinkage by the moment of reaching 1200 °C was in the range of 1.90 (CR11) and 3.87% (CR18). While maintaining the final temperature, the composites mainly exhibited a reduction in length of an additional 0.03 (CR4) up to 3.96% (CR5). The exceptions are noticed in the case

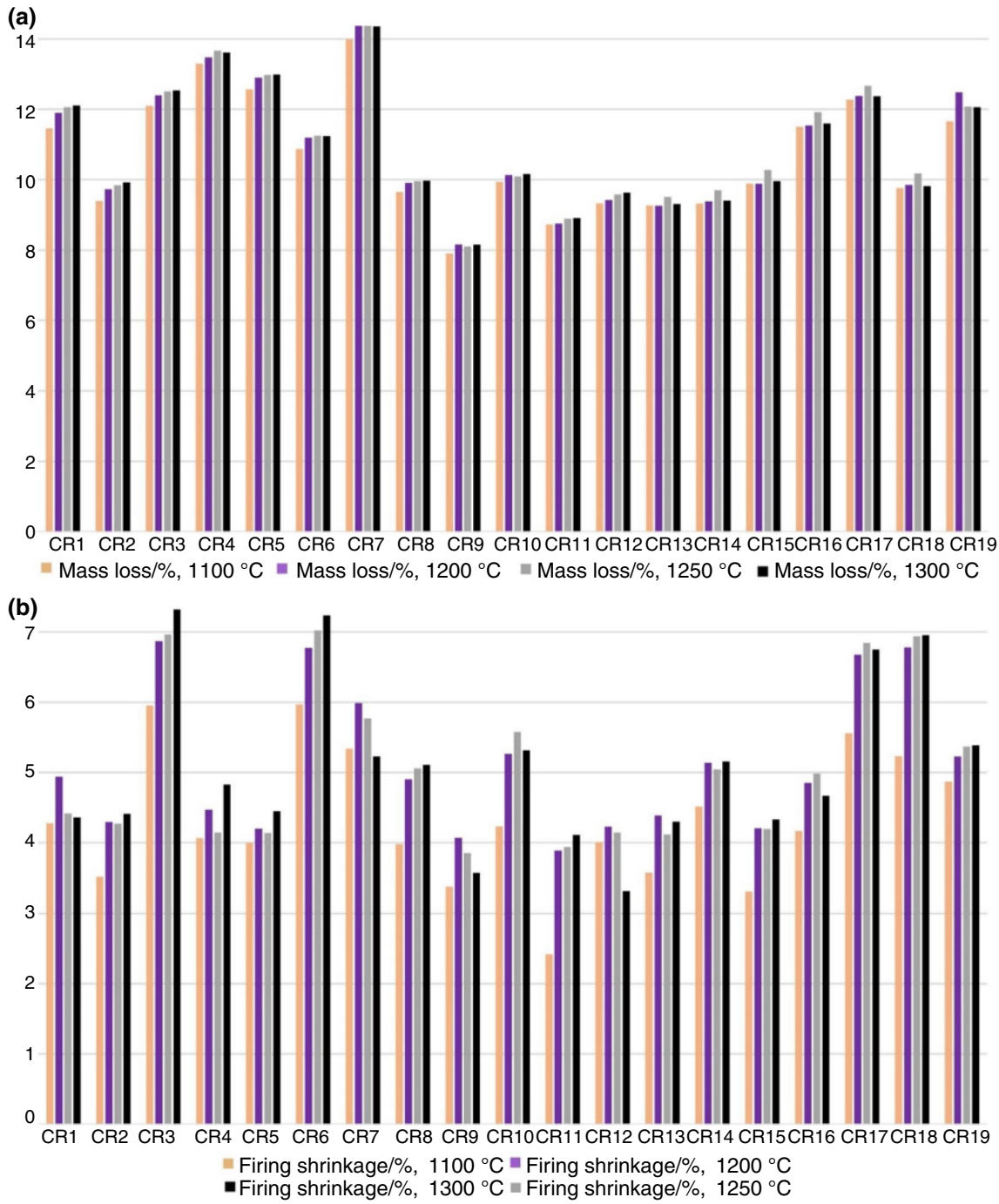

Fig. 5 **a** Mass loss and **b** firing shrinkage in the 1100–1300 °C range

of CR5 and CR16 which showed the opposite behavior and spread by 2.54 and 3.66%, respectively. The total shrinkage of the composites after cooling ranged from 4.67 (CR15) to 8.65% (CR18). The firing regime, especially at high temperatures, was too fast in the case of CR5 and CR16, due to high organic matter content and the occurrence of the entrapped air [26]. The final dimensions are also affected by the mineralogical content of the composites, the size and morphology of the clay minerals particles, the share of fluxes, the formation of gases and the expansive formation of cristobalite [1, 28]. The total shrinkage was mainly related to the content of kaolinite in the composites. Since the composites CR5 and CR16 experienced bloating during firing, they are not considered suitable to be used as refractory materials if fired following a fast regime [26, 28, 38].

Table 4 Water absorption by boiling (WA_b) and in the vacuum (WA_v)

	WA_v/%, 1100 °C	WA_b/%, 1100 °C	WA_v/%, 1200 °C	WA_b/%, 1200 °C	WA_v/%, 1250 °C	WA_b/%, 1250 °C	WA_v/%, 1300 °C	WA_b/%, 1300 °C
CR1	7.19	7.08	4.97	4.50	4.62	3.84	4.68	3.99
CR2	6.64	6.30	4.20	3.48	3.27	2.34	3.18	2.02
CR3	7.54	7.04	5.12	4.30	4.50	3.96	4.45	3.69
CR4	9.02	8.94	7.38	7.22	6.93	6.73	6.77	6.46
CR5	7.84	7.88	6.35	6.11	6.08	5.57	6.31	5.40
CR6	5.69	5.31	3.45	2.98	3.17	2.63	2.94	2.47
CR7	6.95	6.71	5.41	4.70	4.77	3.97	4.82	3.82
CR8	7.52	7.26	5.19	4.77	4.24	3.67	4.17	3.57
CR9	6.33	6.04	3.23	2.48	2.53	1.62	2.59	1.33
CR10	6.47	6.13	3.85	3.47	3.16	2.55	2.79	2.22
CR11	8.39	8.20	5.03	4.77	4.28	3.83	3.58	2.95
CR12	5.37	5.26	2.51	1.50	3.09	0.98	3.51	2.37
CR13	6.09	6.09	3.70	3.21	2.77	2.21	2.50	1.53
CR14	5.53	5.37	3.21	2.79	2.38	1.70	2.41	1.85
CR15	6.68	6.68	4.07	3.77	3.86	3.52	3.78	3.29
CR16	7.44	7.25	5.66	5.43	5.05	4.78	4.88	4.61
CR17	6.17	5.85	3.99	3.52	3.61	2.90	3.81	3.02
CR18	6.39	5.97	2.83	2.05	1.88	1.09	1.42	0.82
CR19	6.51	6.05	5.33	5.51	5.13	4.97	4.79	4.85
Min.*	5.37	5.26	2.51	1.50	1.88	0.98	1.42	0.82
Max	9.02	8.94	7.38	7.22	6.93	6.73	6.77	6.46
Aver	6.83	6.60	4.50	4.03	3.96	3.31	3.86	3.17
St.Dev	0.96	1.00	1.26	1.44	1.30	1.54	1.35	1.47

**Min.* minimum, *Max.* maximum, *Aver.* average, *SD* standard deviation

Refractoriness

As the most important indicator of the usability of tested composites in the production of refractory bricks, tests according to Seger cones (SC) were performed [9, 10]. The melting temperatures and SC refractoriness (Fig. 4) classify the composites into low-duty (CR2, CR6, CR9–CR15), low- and medium-duty boundary cases (CR1, CR3, CR5, CR8, CR18), medium-duty (CR7, CR16, CR19) and high-duty (CR17) refractories [30]. The melting temperatures were between 1581 °C (SC 26, CR9) and 1718 °C (SC 32, CR17). The composite that showed the lowest refractoriness (CR9) contained the highest total amount of fluxes presented as oxides (63.32%, Table 1), and among the lowest quantities of total clay minerals, as from the XRD analyses (51.70%, Table 2). The CR17 fused somewhat below the melting temperature of pure kaolinite [39]. Since most of the refractoriness is determined as above 1585 °C [26], the materials are considered adequate for the production of refractories except for the sample CR9. The correlation analysis (Table 6 in Appendix) revealed the highest contribution of Al_2O_3 (positive), SiO_2 (negative), K_2O (negative) and Fe_2O_3 (negative) to the refractoriness. The key impact on the refractoriness is the quantity of kaolinite [2].

Properties of the dried and fired samples

Behavior during shaping and drying

The important properties and appearance of the manually formed and hydraulically pressed samples (Table 8 in Appendix) indicated stable green products. According to the coefficient of plasticity, composite samples are classified into moderate (CR15, CR13, CR1, CR2, CR16, CR10, CR11, CR14 and CR9), good (CR7, CR12, CR5, CR4, CR8 and CR19) and highly plastic (CR6, CR3, CR17 and CR18) raw materials. Following the position of the critical point on Bigot's curves (ΔSk—shrinkage and ΔGk—mass loss in the critical point), most of the composites are classified into materials sensitive to drying ($7\% \leq \Delta Gk \leq 10\%$), and some of them belong to the highly sensitive group ($\Delta Gk \geq 10\%$), and those were CR8, CR10, CR18, CR17, CR6 and CR3. The plasticity and sensitivity to drying depended mostly on the kaolinite contents and clay-sized fraction quantity, which was following the previous studies [12]. The shrinkage of the dried hand-shaped samples at 105 °C varied considerably (from 4.13 to 9.94%) and was highly defined by the content of clay-sized fractions and shaping moisture that was needed to obtain plastic bodies.

Table 5 Compressive strength (CS) and modulus of rupture (MR)

	CS/MPa, 1100 °C	CS/MPa, 1200 °C	CS/MPa, 1250 °C	CS/MPa, 1300 °C	MR/MPa, 1100 °C	MR/MPa, 1200 °C	MR/MPa, 1250 °C	MR/MPa, 1300 °C
CR1	65	75.2	78.53	75.79	24.2	36.63	40.55	36.16
CR2	56.17	73.86	76.57	83.86	27.26	40.06	43.62	45.65
CR3	69.39	75.42	93.19	97.86	32.53	41.55	44.51	48.67
CR4	41.02	69.71	86.79	91.66	16.5	22.94	26.59	27.16
CR5	49.76	65.78	76.87	89.43	24.35	25.28	27.58	31.51
CR6	64.03	86.33	96.74	134.43	38.13	40.71	43.15	46.36
CR7	44.52	55.43	68.81	66.34	29.42	36.43	37.44	34.54
CR8	63.88	72.8	90.12	107.53	30.8	34.67	35.07	37.55
CR9	57.47	89.29	99.49	130	32.8	34.97	35.44	37.7
CR10	37.72	56.18	67.82	77.99	28.09	42.7	44.96	48.16
CR11	47.49	76.09	85.83	91.93	18.27	26.81	30.7	33.28
CR12	52.12	64.68	84.18	81.89	35.89	42.69	46.53	38.53
CR13	56.29	78.96	92.63	129.77	28.86	35.05	37.91	40.81
CR14	43.75	70.23	92.44	85.88	30.66	35.58	38.87	35.85
CR15	38.8	51.28	59.44	75.97	22.92	32.05	33	36.8
CR16	47.15	56.02	63.95	76.51	24.99	26.14	32.48	36.18
CR17	40.87	51.67	64.89	62.31	36.36	38.19	39.07	38.79
CR18	51.9	78.12	95.4	130.28	41.69	44.4	50.97	53.6
CR19	56.78	61.12	71.73	65.46	27.86	29.91	30.15	29.34
Min.*	37.72	51.28	59.44	62.31	16.50	22.94	26.59	27.16
Max	69.39	89.29	99.49	134.43	41.69	44.40	50.97	53.60
Aver	51.80	68.85	81.34	92.36	29.03	35.09	37.82	38.77
St.Dev	9.55	11.27	12.53	23.36	6.47	6.43	6.76	6.95

**Min.* minimum, *Max.* maximum, *Aver.* average, *SD* standard deviation

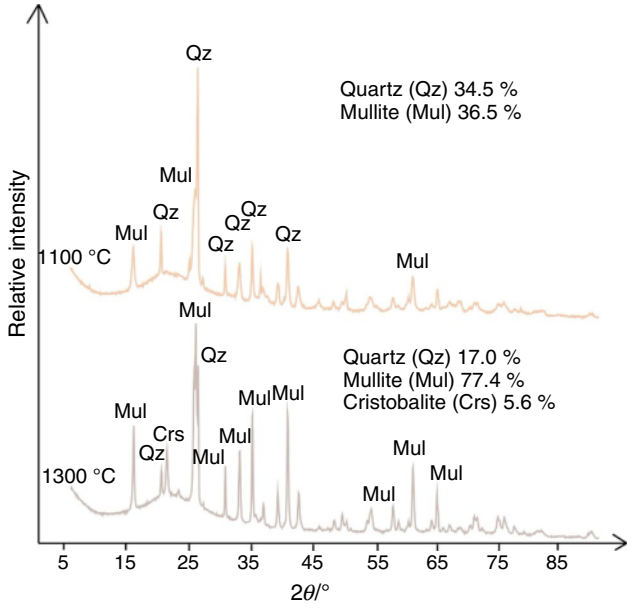

Fig. 6 Mineralogical composition of the most refractory sample fired at 1100 and 1300 °C

The highest shrinkage was observed in the CR6, which contained the highest clay fraction content and among the highest clay minerals contents (Table 2). Concerning compressive strength and modulus of rupture (Table 8 in Appendix), dry specimens were of satisfactory quality in terms of stability during handling. The maximal dry strength was in the case of CR1, due to the highest content of sand fraction (Table 3) [30]. The lower share of clay minerals negatively influenced the mechanical strength of the dry products, as seen previously [40].

Behavior related to the firing process

The lowest loss on ignition (Fig. 5) at all the firing temperatures is observed in CR9 (7.90%) and the highest in CR7 (14.37%), which is consistent with the results presented in Figs. 1 and 4, and depended mostly on the total clay minerals contents, and somewhat on organic matter quantity. The firing shrinkage of the composites varied in the range of 2.42% (at 1100 °C) to 7.32% (at 1300 °C), which is considered satisfactory in refractory clays [26]. The shrinkage was the lowest in CR11 and highest in CR3 and CR6 in all the firing temperatures. In most of the composites, the firing shrinkage

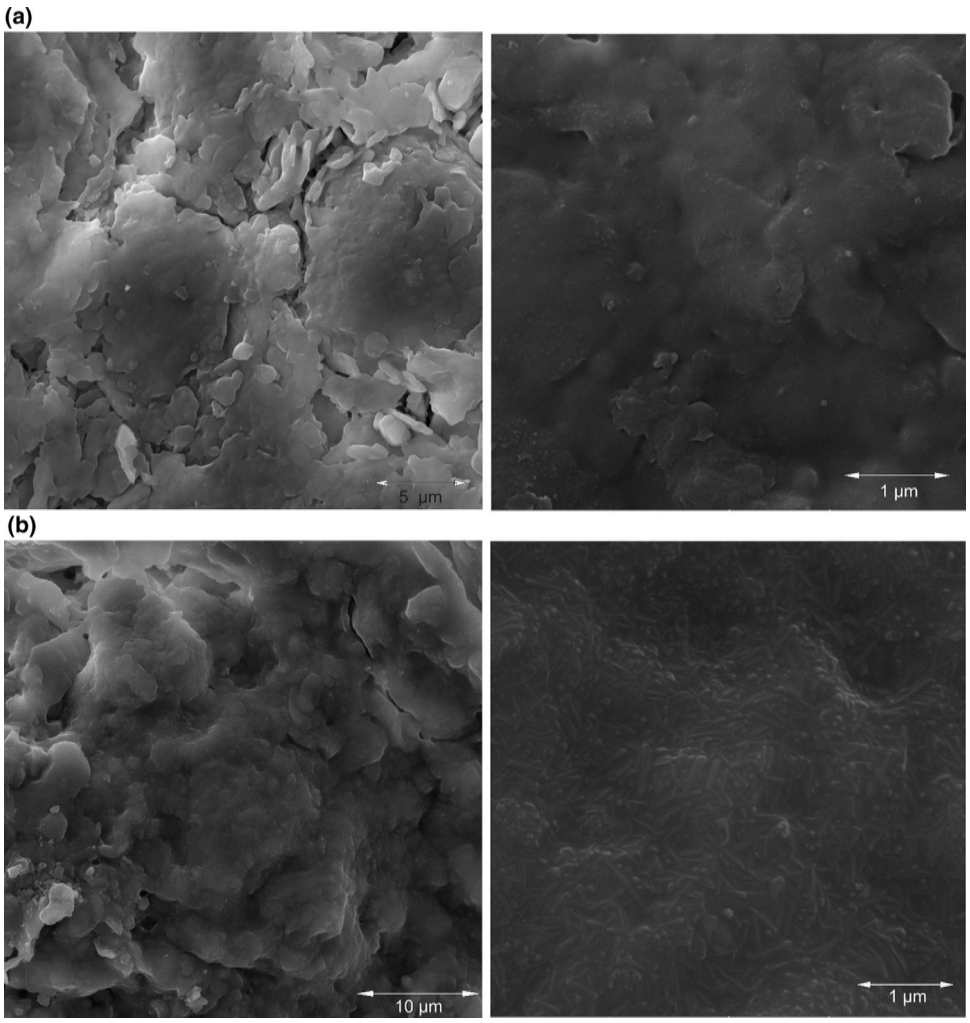

Fig. 7 Microstructure of the most refractory sample fired at **a** 1100 and **b** 1300 °C

did not increase linearly with the temperature. The extent of mass loss during firing is considered dependent on many compositional features of materials [30], but correlation analysis (Table 9 in Appendix) revealed that the most influential factors in the studied composites were the content of kaolinite (positive) and quartz (negative). Firing shrinkage in the tested composites was strongly affected by kaolinite content and shaping moisture (Table 9 in Appendix), which is also seen in other studies [41]. By firing at 1300 °C, quartz did not show a statistically significant correlation with firing shrinkage.

Water absorption of the composite samples is determined by two methods (Table 4). The results mainly showed a decrease in water absorptions and a raise in mechanical properties (Table 5) with the firing temperature due to sintering. Some exceptions are noticed after firing at 1300 °C when the water absorption raised and mechanical properties dropped when compared to the results gained at 1250 °C. This was the case in CR1, CR12, CR14, CR17 and CR19, possibly due to the higher quantities of K_2O (above 1.5%). The somewhat increased water absorption must not be a drawback, since the porosity is necessary for efficient binding during the installation of the product [26]. The water absorption by boiling ranged from 0.82–8.94% and in vacuum 1.42–9.02%. The highest water absorption was determined in the CR4 at 1100 °C and the lowest in the CR18 at 1300 °C. The results were similar to the ranges for refractories studied previously [42]. The water absorption for the tested samples generally showed lower values compared to a chamotte [43] or ceramic tiles [7] and higher than traditional building bricks [44]. The constraint for compressive strength above 20 MPa [45] or above 34 MPa [46] in refractory bricks was satisfied in all the composites and firing temperatures (Table 4). The flexural strengths obtained in all the cases were higher than previously reported [19, 41]. According to the correlation analysis (results not presented), the flexural strength was statistically significantly negatively influenced by the high content of hematite.

Additionally, the mineralogical composition of the most refractory sample (CR17) fired at 1100 °C and

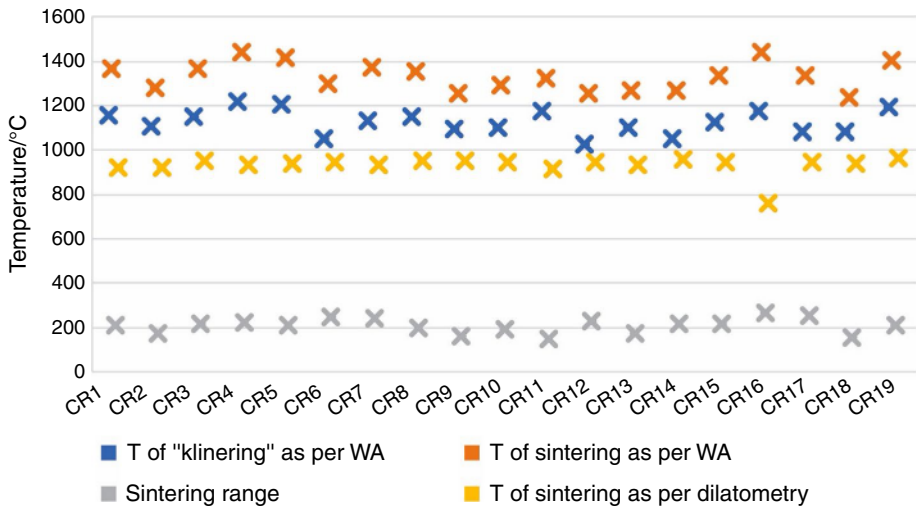

Fig. 8 Sintering temperature and sintering range

1300 °C was done (Fig. 6). At these temperatures, illite–mica has already degraded to an amorphous phase. A noticeable difference was observed by a drop in the quartz concentration, which is dramatically reduced around 1100 °C [47]. At roughly 1200 °C, spinel completely decomposes, causing cristobalite to crystallize from a silica-rich amorphous phase and the abrupt development of mullite crystals [48]. The content of residual quartz was reduced by half, while cristobalite is detected at the higher temperature (1300 °C). At the same time, the share of mullite significantly increased which improved the mechanical strength of the fired samples (Table 5). The microstructure of the most refractory sample (CR17) revealed the differences in the strength of the material (Fig. 7). The sample fired at 1100 °C showed more pronounced cracks and very low content of mullite crystals while preserving some of the initial hexagonally shaped kaolinite particles. On the other hand, after firing at 1300 °C more pronounced mullite needle-like crystals appeared fused in the glassy phase, improving the mechanical strength. Strength growth was positively impacted by the complete wetting of the crystalline phases and the lesser cracks as a result of the crystalline and glassy phases' volume expansion.

The sintering range, as determined by the method explained previously [7] (Fig. 8), was satisfying and varied from 150 (CR11) to 266 °C (CR16). The range was higher than in raw materials used in ceramic tile production [7]. The sintering range in the raw composites was wider with a higher quantity of kaolinite, which was contrary to the previous findings [38]. The sintering range in this data set showed correlations to the content of SiO_2 and loss on ignition, and not the K_2O content as reported previously [28, 47]. The sintering temperature was highly dependent on loss on ignition, K_2O content [30, 38], SiO_2 and Al_2O_3 content. The higher sintering temperature can appoint the materials closer to commercial kaolin [40].

Color of the dry and fired samples

The final color of refractories mainly does not limit their application, except in the case of facing bricks. However, the color is determined to follow the possible indication of the raw material composition, reactions during firing and important characteristics of the fired products. The $L^*a^*b^*$ values (Fig. 9) are presented for the dry and fired products. In the case of dry (green) refractories, the lowest L^* was found in the samples containing the most organic matter (CR16), which bloated when recorded using a dilatometer. The samples mostly showed the highest L^* values when fired at 1100 °C, after which they are mostly darker, being the darkest after firing at 1300 °C, which was also obtained in the other studies [49].

The red tonality was most intensive at 1200 °C, while the lowest a^* values in the fired samples were at 1300 °C. The cause of this phenomenon may be the incorporation of Fe^{3+} ions into the structure of mullite by altering Al^{3+} [5] or the reduction to Fe^{2+} at temperatures above 1200 °C. On the other side, some ilmenite may be formed when firing at about 1200 °C, thus producing a dark color [30, 49]. The lowest a^* was for dry products. The yellow hue was generally the most intense in samples fired at 1100 °C due to the white cristobalite grains formation and most often the lowest at 1300 °C. Some of the samples had a similar intensity of red and yellow shades after firing at 1250 and 1300 °C (CR2, CR3, CR5, CR8, CR11, CR12). ΔE^* relative to the reference dry samples [41, 50] generally decreased with temperature (Fig. 10 in Appendix). The observed differences may be caused by the appearance of dark round pores of the initial goethite particles position [44], as

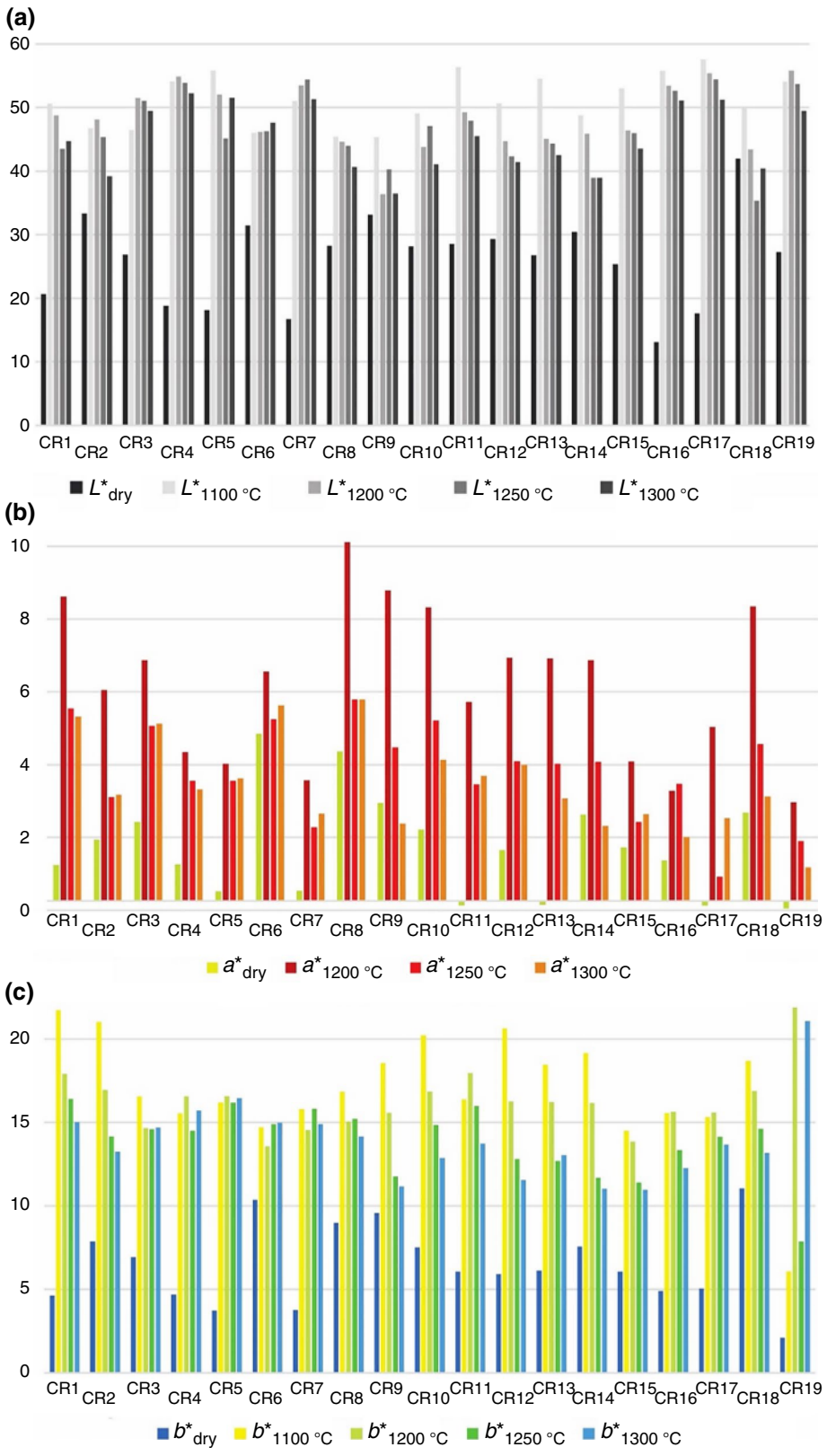

Fig. 9 $L^*a^*b^*$ values in dry samples and samples fired in an 1100–1300 °C range

shown in Fig. 11 in Appendix. Round metallic iron particles were also included in the composites and were spread in a vitreous phase. The surface of the samples appeared slightly rough under an optical microscope, thus indicating the open porosity necessary for binding the pieces together. The SiO_2/Al_2O_3 mass ratio in the 1.72–2.32 range (Table 1) implied the palest fired color [22] in the case of CR17 and the darkest in CR9.

The correlation analysis, shown in Table 10 (Appendix), revealed the statistically significant influence of the color and properties of the fired specimens. Thus, the lightness of the green samples and the b^* component was highly influential to the modulus of rupture and compressive strength at all the firing temperatures examined. Also, $L^*a^*b^*$ coordinates of the bodies fired at 1100 °C had a causal relationship with the modulus of rupture. Among the fired samples, the compressive strength was mainly influenced by L^* and a^* coordinates. Refractoriness was determined as mostly dependent on the lightness of both green and fired specimens. The linear relationships between the here studied parameters should be further analyzed in the future, thus obtaining a mathematical model which would predict the quality of the products based on their color.

Additional comments on the usability of tested composites

The tested composites are determined as suitable for lining ceramic kilns or the parts of wagons. They can also be used for furnaces in the glass industry [1, 5]. To avoid bloating of the product during firing, a slower firing regime than that used in this study should be applied, to ensure complete gas evolution [2]. The tested composites also could be used in a smaller percentage as one of the components for the production of ceramic tiles due to the high content of organic matter (high loss on ignition) and the tendency to swell during the fast-firing process used in modern production. Besides, they can be used as one of the components for the production of sewage pipes and brick products.

To obtain chamotte, clinker or facing brick, quartz or carbonates should be added to these materials [27, 28, 49]. Besides, ceramic coatings could be used to improve the energy efficiency of the tested composites. In addition, these composites can be used in a fired state as an additive to the mixture for the production of chamotte or chamotte flour [49]. The opposite can be done by mixing 0.5 mm to several mm fractions of a chamotte, so even higher-quality refractory products could be obtained in these composites [1].

Each of these applications would require additional testing, such as thermal shock, mechanical strength at elevated temperatures and thermal expansion [5].

Conclusions

This study aimed to present the results of 19 raw refractory materials composites and the possibility of their industrial application. From this investigation, the following conclusions can be drawn:

(1) The chemical analysis showed variations in the contents of SiO_2 (48.85–57.21%), Al_2O_3 (24.70–29.18%) and the sum of fluxing oxides (2.41–4.46%).
(2) The mineralogical analysis revealed that the contents of quartz were in the range of 20.50–45.80%, kaolinite 23.10–45.80%, illite–mica 18.40–33.70% and hematite 0.40–1.00%.
(3) Thermal analyses confirmed the XRD analysis, showing that the samples contained high levels of organic matter and clay minerals, which is seen in the most intensive mass loss by the firing in the 400–600 °C range. Some of the composites experienced bloating or entrapped air at the surface by a fast-firing regime.
(4) Seger cones refractoriness test revealed that the composites may be used as low- to high-duty refractories, which is mostly dependent on the contents of total clay minerals and fluxes.
(5) The materials were satisfying in terms of hydraulic pressing and had a stable shape when dry. After firing in the range of 1100–1300 °C, firing shrinkage was in the range of 2.42–7.32%, water absorption 1.42–2.02% and modulus of rupture 16.5–53.6 MPa.
(6) Mineralogical composition and microstructural appearance of the fired sample containing the highest share of kaolinite revealed the partly transformation of quartz to cristobalite and kaolinite to mullite, while strengthening the matrix mechanical strength after firing at 1300 °C.
(7) The $L^*a^*b^*$ of the composites revealed interesting relationships to the mineral transformations during firing and properties of the products.

Based on all the above, it was concluded that the tested materials can be used alone or in a combination with quartz or carbonates as refractory materials. Besides, they can be utilized to produce chamotte or mixed with other clays in ceramic tiles production.

Appendix

See Appendix Tables 6, 7, 8, 9 and 10 and Figs. 10 and 11.

Table 6 Correlation coefficients between oxide content in refractory raw materials with statistical significance

	SiO_2/%	Al_2O_3/%	Fe_2O_3/%	CaO/%	MgO/%	Na_2O/%	K_2O/%	SO_3/%	P_2O_5/%	MnO/%	TiO_2/%
Refractoriness/°C	− 0.799**	0.893**	− 0.506*	0.266	− 0.265	− 0.440	− 0.579*	0.256	0.370	− 0.270	− 0.455
LOI/%***	− 0.969**	0.792**	− 0.158	0.295	− 0.246	− 0.541*	− 0.782**	0.278	0.264	− 0.264	− 0.460*
SiO_2/%		− 0.838**	0.187	− 0.293	0.134	0.492*	0.692**	− 0.368	− 0.332	0.192	0.552*
Al_2O_3/%			− 0.583**	0.024	− 0.357	− 0.463*	− 0.604*	0.127	0.077	− 0.107	− 0.403
Fe_2O_3/%				0.437	0.144	0.025	− 0.047	0.179	0.271	0.085	0.043
CaO/%					− 0.020	− 0.209	− 0.528*	0.542*	0.447	− 0.490*	− 0.137**
MgO/%						0.376	0.400	0.472*	0.312	− 0.093	− 0.038
Na_2O/%							0.519*	0.216	− 0.272	0.262	0.195
K_2O/%								0.280	− 0.146	0.406	0.049
SO_3/%									0.257	− 0.361	− 0.202
P_2O_5/%										− 0.126	− 0.163
MnO/%											− 0.115

*Significant correlation at $p < 0.05$ level

**Significant correlation at $p < 0.01$ level

****LOI* Loss on ignition

Table 7 Correlation coefficients between the contents of minerals in refractory raw materials with statistical significance

	Kaolinite/%	Illite–mica/%	Hematite/%	Anatase/%	Mutinaite/%	Faujasite/%	Magnesian calcite/%
Quartz/%	− 0.764**	− 0.032	0.145	− 0.604**	− 0.200	− 0.040	− 0.356
Kaolinite/%		− 0.564*	− 0.312	0.443	0.067	− 0.281	0.023
Illite–mica/%			0.316	0.041	− 0.225	0.486*	0.481*
Hematite/%				0.003	− 0.0248	− 0.068	0.024
Anatase/%					0.065	0.169	0.505*
Mutinaite/%						− 0.104	− 0.258
Faujasite/%							0.655**

*Significant correlation at $p < 0.05$ level

**Significant correlation at $p < 0.01$ level

Table 8 Properties during drying of manually and hydraulically formed samples

	Manually formed samples						Hydraulically formed tiles				
	Shaping moisture/%	Plasticity coefficient (Pfefferkorn)	*ΔSk**/% (Bigot's curve)	*ΔGk**/% (Bigot's curve)	Drying shrinkage/%	Dry compressive strength/MPa	Shaping moisture/%	Dry modulus of rupture/MPa	*L**	*a**	*b**
CR1	19.48	22.70	4.97	8.71	5.50	4.48	4.00	3.34	20.66	0.99	4.64
CR2	21.02	22.80	6.13	9.75	6.22	3.10	4.00	2.87	33.31	1.69	7.89
CR3	27.27	32.30	6.44	12.26	7.76	3.66	4.00	2.62	26.85	2.18	6.96
CR4	19.82	26.40	4.94	8.77	5.28	3.02	4.00	2.40	18.81	1.01	4.70
CR5	20.18	25.70	5.24	9.36	6.10	4.22	4.00	2.66	18.15	0.27	3.73
CR6	25.41	30.60	6.31	12.13	9.94	3.74	4.00	2.43	31.44	4.59	10.37
CR7	18.85	25.10	4.18	9.00	5.19	3.07	4.00	2.21	16.74	0.28	3.77
CR8	22.91	27.60	4.46	10.57	6.06	3.77	4.00	2.15	28.23	4.12	9.00
CR9	19.48	24.60	4.66	7.72	5.28	3.09	4.00	2.40	33.14	2.70	9.58
CR10	19.86	23.00	4.00	10.77	5.50	2.42	4.00	2.86	28.15	1.97	7.52
CR11	19.42	23.30	4.75	8.65	5.17	3.73	4.00	3.90	28.52	− 0.12	6.07
CR12	21.05	25.40	3.78	8.63	5.05	3.09	4.00	2.79	29.30	1.40	5.92
CR13	18.02	20.50	4.06	7.87	5.05	4.19	4.00	3.13	26.78	− 0.11	6.14
CR14	19.45	24.10	2.63	6.34	5.15	3.14	4.00	2.87	30.43	2.38	7.58
CR15	17.43	20.10	4.28	7.15	4.13	3.91	4.00	3.39	25.34	1.47	6.07
CR16	16.69	22.80	3.70	9.93	5.35	3.52	4.00	2.66	13.10	1.11	4.93
CR17	26.76	32.40	5.53	11.93	5.92	2.68	4.00	2.15	17.63	− 0.13	5.05
CR18	26.60	33.00	5.76	11.24	6.96	2.68	4.00	1.79	41.94	2.43	11.04
CR19	21.12	29.90	4.94	9.20	6.25	3.64	4.00	2.85	27.22	− 1.10	− 0.32

**ΔSk* shrinkage in the critical point, *ΔGk* mass loss in the critical point

Table 9 Correlations of mineralogy and shaping moisture to some properties of the fired refractories

	Loss on ignition/%				Firing shrinkage/%			
	1100 °C	1200 °C	1250 °C	1300 °C	1100 °C	1200 °C	1250 °C	1300 °C
Quartz/%	− 0.642**	− 0.636**	− 0.650**	− 0.634**	− 0.658**	− 0.574*	− 0.490*	− 0.415
Kaolinite/%	0.631**	0.601**	0.627**	0.587*	0.740**	0.761**	0.729**	0.696**
Illite–mica/%	0.255	− 0.201	− 0.234	− 0.178	− 0.238	− 0.322	− 0.380	− 0.396
Hematite/%	0.256	0.270	0.240	0.269	− 0.276	− 0.356	− 0.378	− 0.404
Anatase/%	0.536*	0.554*	0.541*	0.548*	0.514*	0.480*	0.442	0.443
Mutinaite/%	0.110	0.081	0.107	0.065	− 0.198	− 0.266	− 0.289	− 0.328
Faujasite/%	− 0.011	0.032	0.027	0.057	− 0.131	− 0.152	− 0.225	− 0.206
Magnesian calcite/%	0.458	0.507*	0.482*	0.527*	0.254	0.126	0.048	0.135
Shaping moisture/%	0.132	0.146	0.140	0.139	0.705**	0.784**	0.798**	0.813**

*Significant correlation at $p < 0.05$ level

**Significant correlation at $p < 0.01$ level

Table 10 Correlations of $L^*a^*b^*$ and properties of the fired products

	L^*_{dry}	a^*_{dry}	b^*_{dry}	$L^*_{1100\,°C}$	$a^*_{1100\,°C}$	$b^*_{1100\,°C}$	$L^*_{1200\,°C}$	$a^*_{1200\,°C}$	$b^*_{1200\,°C}$	$L^*_{1250\,°C}$	$a^*_{1250\,°C}$	$b^*_{1250\,°C}$	$L^*_{1300\,°C}$	$a^*_{1300\,°C}$	$b^*_{1300\,°C}$
$MR_{1100\,°C}$/MPa	0.506*	0.471*	0.608**	− 0.437	0.487*	0.140	− 0.384	0.421	− 0.344	− 0.393	,1606	− 0.172	− 0.292	0.121	− 0.212
$MR_{1200\,°C}$/MPa	0.594**	0.403	0.546*	− 0.580*	0.560**	0.481*	− 0.429	0.551*	− 0.141	− 0.368	0.276	− 0.076	− 0.462	0.292	− 0.238
$MR_{1250\,°C}$/MPa	0.624**	0.365	0.560*	− 0.498*	0.507*	0.493*	− 0.379	0.486*	− 0.041	− 0.386	0.286	− 0.065	− 0.424	0.234	− 0.243
$MR_{1300\,°C}$/MPa	0.608**	0.372	0.552*	− 0.491*	0.486*	0.458	− 0.383	0.465	− 0.082	− 0.387	0.309	− 0.065	− 0.404	0.255	− 0.245
$CS_{1100\,°C}$/MPa	0.2993	0.466	0.376	− 0.578*	0.538*	0.224	− 0.258	0.536*	− 0.102	− 0.269	0.643**	0.235	− 0.171	0.677**	,2731
$CS_{1200\,°C}$/MPa	0.608**	0.453	0.608**	− 0.521*	0.501*	0.258	− 0.528*	0.570*	0.142	− 0.522*	0.608**	0.042	− 0.411	0.375	0.111
$CS_{1250\,°C}$/MPa	0.621**	0.478*	0.614**	− 0.506*	0.532*	0.173	− 0.498*	0.589**	0.052	− 0.503*	0.607**	− 0.007	− 0.358	0.382	0.104
$CS_{1300\,°C}$/MPa	0.648**	0.478*	0.648**	− 0.425	0.453	0.217	− 0.661**	0.580**	− 0.046	− 0.635**	0,568**	− 0.176	− 0.451	0.318	− 0.095
Refractoriness T/°C	− 0.503*	− 0.187	− 0.328	0.280	− 0.196	− 0.293	0.761**	− 0.318	− 0.050	0.530*	− 0.329	0.487*	0.668**	0.049	0.603

*Significant correlation at $p < 0.05$ level

MR modulus of rupture, *CS* compressive strength

**Significant correlation at $p < 0.01$ level

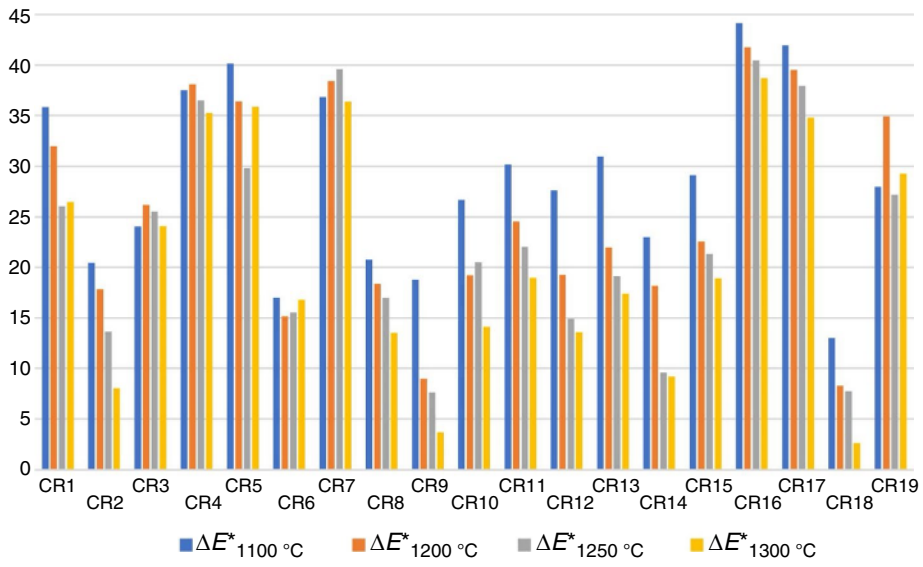

Fig. 10 ΔE^* relative to the reference dry samples

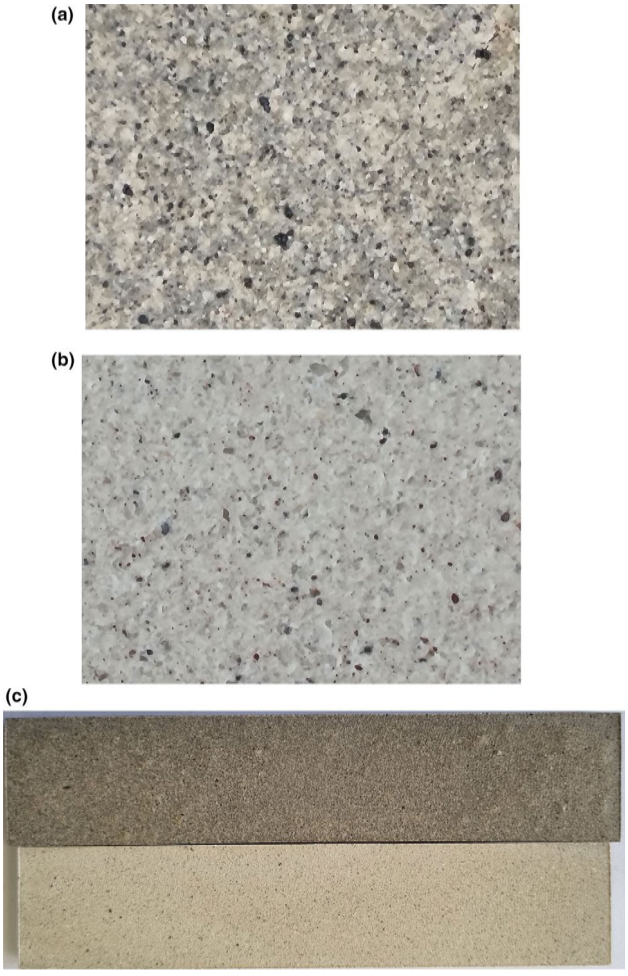

Fig. 11 Microscopic (magnification 13x) and macroscopic appearance of the darkest (CR9) and the lightest composite (CR17)

Supplementary Information The online version contains supplementary material available at https://doi.org/10.1007/s10973-022-11848-w.

Acknowledgements The presented work is supported by the Ministry of Education, Science and Technological Development of the Republic of Serbia (Contract No. 451-03-68/2022-14/200012 and Contract No. 451-03-68/2022-14/200287), and forms part of a collaboration between the Institute for Testing of Materials IMS and Innovation Centre of the Faculty of Technology and Metallurgy, University of Belgrade.

Author's contribution The study conception, methodology, design and writing the first draft of the manuscript were performed by Milica V. Vasić. Material preparation, data collection, visualization, analysis and discussion were also done by Milica V. Vasić. Visualization and discussion are done by Lidija Radovanović. Statistical analysis was performed by Lato Pezo. Conceptualization, methodology and supervision were the tasks done by Zagorka Radojević. The first draft of the manuscript was written by Milica V. Vasić and all authors commented on previous versions of the manuscript. All authors read and approved the final manuscript.

Declarations

Conflict of interest The authors declare that they have no known competing financial interests or personal relationships that could have appeared to influence the work reported in this paper.

References

1. Pountouenchi A, Njoya D, Njoya A, Rabibisao D, Mache JR, Yongue RF, Njopwouo D, Fagel N, Pilate P, Van Parys L. Characterization of Foumban (West Cameroon) region's clays and suitability evaluation for refractory bricks manufacturing. Clay Miner. 2018. https://doi.org/10.1180/clm.2018.32.
2. Patterson SH, Hosterman JW, Huddle JW. Geology and refractory clay deposits of the Haldeman and Wrigley Quadrangles. Kentucky Geol Surv Bull. 1962. https://doi.org/10.3133/b1122F.

3. Vasić MV, Pezo LL, Zdravković JD, Vrebalov M, Radojević Z. Thermal, ceramic and technological properties of clays used in production of roofing tiles—principal component analysis. Sci Sinter. 2018. https://doi.org/10.2298/SOS1804487V.
4. Vasić MR, Vasić MV. Optimize, upgrade or invest in a novel dryer?—A brick factory case study. Int J Manuf Econ Manag. 2021. https://doi.org/10.54684/ijmem.2021.1.2.62.
5. Schacht CA. Refractories handbook. Pennsylvania: Schacht Consulting Services Pittsburgh; 2004.
6. SRPS U.B1.018. Testing of soils—determination of particle size distribution. Serbia: Institute for Standardization of Serbia; 2005.
7. Vasić MV, Pezo L, Vasić MR, Mijatović N, Mitrić M, Radojević Z. What is the most relevant method for water absorption determination in ceramic tiles produced by illitic-kaolinitic clays? The mystery behind the gresification diagram. Bol Soc Esp Ceram. 2022. https://doi.org/10.1016/j.bsecv.2020.11.006.
8. Hillier S. Accurate quantitative analysis of clay and other minerals in sandstones by XRD: Comparison of a Rietveld and reference intensity ratio (RIR) method and the importance of sample preparation. Clay Miner. 2000. https://doi.org/10.1180/000985500546666.
9. EN 993-12. Methods of test for dense shaped refractory products—part 12: determination of pyrometric cone equivalent (refractoriness). Serbia: Institute for Standardization of Serbia; 1997.
10. EN 993-13. Methods of test for dense shaped refractory products—part 13: specification for pyrometric reference cones for laboratory use. Serbia: Institute for Standardization of Serbia; 1995.
11. ASTM C24-09. Standard test method for pyrometric cone equivalent (PCE) of fireclay and high-alumina refractory materials. West Conshohocken: ASTM International; 2018.
12. Arsenović M, Pezo L, Mančić L, Radojević Z. Thermal and mineralogical characterization of loess heavy clays for potential use in brick industry. Thermochim Acta. 2014. https://doi.org/10.1016/j.tca.2014.01.026.
13. de la Casa JA, Lorite M, Jiméndez J, Castro E. Valorisation of wastewater from two-phase olive oil extraction in fired clay brick production. J Haz Mater. 2009. https://doi.org/10.1016/j.jhazmat.2009.03.095.
14. Pfefferkorn KK. Ein beitrag zur bestimmung der plastizität in tonen und kaolinen. Sprechsaal. 1924;57(25):297–9.
15. ASTM C20-00. Standard test methods for apparent porosity, water absorption, apparent specific gravity, and bulk density of burned refractory brick and shapes by boiling water. West Conshohocken: ASTM International; 2015.
16. SRPS EN ISO 10545-3. Ceramic tiles—part 3: determination of water absorption, apparent porosity apparent relative density and bulk density. Serbia: Institute for Standardization of Serbia; 2018.
17. McGuire RG. Reporting of objective color measurements. HortScience. 1992;27:1254–5.
18. Pavlova IA, Getman AA, Farafontova EP. Technogenic raw materials in high-alumina chamotte production. IOP Conf Ser: Mater Sci Eng. 2020. https://doi.org/10.1088/1757-899X/969/1/012031.
19. Haddar AE, Manni A, Azdimousa A, El Hassani I-EEA, Bellil A, Sadik C, Fagel N, El Ouahabi M. Elaboration of a high mechanical performance refractory from halloysite and recycled alumina. Bol Soc Esp Ceram V. 2020; https://doi.org/10.1016/j.bsecv.2019.08.002
20. ISO 10081-1:2003(E). Classification of dense shaped refractory products—part 1: alumina-silica. International Organization for Standardization; 2003.
21. Wilder DR, Dodd CM. Some effects of titania on refractory clays. In: 55th annual meeting. New York: The American Ceramic Society; 1953.
22. Garcia-Valles M, Alfonso P, Martínez S, Roca N. Mineralogical and thermal characterization of kaolinitic clays from Terra Alta (Catalonia, Spain). Miner. 2020. https://doi.org/10.3390/min10020142.
23. Fischer P. Some comments on the color of fired clays. ZI. 1984;37:475–83.
24. Dondi M, Raimondo M, Zanelli C. Clays and bodies for ceramic tiles: reappraisal and technological classification. Appl Clay Sci. 2014. https://doi.org/10.1016/j.clay.2014.01.013.
25. Pruett RJ. Kaolin deposits and their uses: Northern Brazil and Georgia, USA. Appl Clay Sci. 2015. https://doi.org/10.1016/j.clay.2016.01.048.
26. Chesters JH. Refractories: production and properties. In: The Iron and Steel Institute, 5th edn. House Press, London; 1973. p. 166–207.
27. SRPS B.F1.010. Refractory materials—refractory clays and kaolins—classification—technical requirements, Institute for Standardization of Serbia, Serbia; 1984.
28. Ramachandran VS, Paroli RM, Beaudoin JJ, Delgado AH. Handbook of thermal analysis of construction materials. New York: Noyes Publications/William Andrew Publishing, Norwich; 2002.
29. Ivanova VP, Kasatov BK, Krasavina TN, Rozinova EL. Термический анализ минералов и горных пород, Министерство геологии СССР, издательство „Недра“, Ленинград (Thermal analysis of minerals and rocks. Ministry of Geology of the USSR, Nedra Publishing House, Leningrad). In: Russian; 1974.
30. Murray HH. Developments in clay science 2. Applied clay mineralogy. Occurrences, processing and application of kaolins, bentonites, palygorskite-sepiolite, and common clays. Elsevier; 2007.
31. Rekik SB, Bouaziz J, Deratana A, Beklouti S. Study of ceramic membrane from naturally occurring-kaolin clays for microfiltration applications. Period Polytech Chem Eng. 2017. https://doi.org/10.3311/PPch.9679.
32. Papadopoulou ND, Lalia-Kantouri M, Kantiranis N, Stratis AJ. Thermal and mineralogical contribution to the ancient ceramics and natural clays characterization. J Therm Anal Calorim. 2006. https://doi.org/10.1007/s10973-005-7173-y.
33. China CL, Ahmada ZA, Sow SS. Relationship between the thermal behaviour of the clays and their mineralogical and chemical composition: example of Ipoh, Kuala Rompin and Mersing (Malaysia). Appl Clay Sci. 2017. https://doi.org/10.1016/j.clay.2017.03.037.
34. Garcia-Valles M, Cuevas D, Alfonso P, Martínez S. Thermal behaviour of ceramics obtained from the kaolinitic clays of Terra Alta, Catalonia, Spain. J Therm Anal Calorim. 2021. https://doi.org/10.1007/s10973-021-11075-9.
35. Ondro T, Húlan T, Al-Shantir O, Csáki Š, Václavů T, Trník A. Kinetic analysis of the formation of high-temperature phases in an illite-based ceramic body using thermodilatometry. J Therm Anal Calorim. 2019. https://doi.org/10.1007/s10973-019-08781-w.
36. Walker RF, Zerfoss S, Holley SF, Gross LJ. Temperature of the inversion in cristobalite. J Res Natl Bur Stand. 1958;61(4):251–61.
37. Plevova E, Vaculikova L, Valovicova V. Thermal analysis and FT-IR spectroscopy of synthetic clay mineral mixtures. J Therm Anal Calorim. 2020. https://doi.org/10.1007/s10973-020-09527-9.
38. Karklit AK, Kaplan FS. On loosening of refractory clays in roasting. Refract Ind Ceram. 2000;41(3–4):96–103.
39. Cheng H, Yang J, Liu Q, He J, Frost RL. Thermogravimetric analysis–mass spectrometry (TG–MS) of selected Chinese kaolinites. Thermochim Acta. 2010. https://doi.org/10.1016/j.tca.2010.05.007.
40. Ligas P, Uras I, Dondi M, Marsigli M. Kaolinitic materials from Romana (north-west Sardinia, Italy) and their ceramic properties. Appl Clay Sci. 1997. https://doi.org/10.1016/S0169-1317(97)00004-5.

41. de Gennaro R, Dondi M, Cappelletti P, Cerri G, de' Gennaro M, Guarini G, Langella A, Parlato L, Zanelli C. Zeolite–feldspar epiclastic rocks as flux in ceramic tile manufacturing. Micropor Mesopor Mater. 2007; https://doi.org/10.1016/j.micromeso.2007.04.023
42. Mokwa JB, Lawal SA, Abolarin MS, Bala KC. Characterization and evaluation of selected kaolin clay deposits in Nigeria for furnace lining application. NIJOTECH. 2019. https://doi.org/10.4314/njt.v38i4.17.
43. Karklit AK, Kakhmurov AV. Burning of briquette to chamotte in a tunnel furnace. Refract. 1994. https://doi.org/10.1007/bf02227385.
44. Bomeni IY, Njoya A, Ngapgue F, Wouatong ASL, Fouateu RY, Kabeyene VK, Fagel N. Ceramic with potential application of ngwenfon alluvial clays (Noun, West Cameroon) in building construction: Mineralogy, physicochemical composition and thermal behaviour. Constr Build Mater. 2018. https://doi.org/10.1016/j.conbuildmat.2018.06.135.
45. Kirabira JB, Wijk G, Jonsson S, Byaruhanga JK. Fireclay refractories from Ugandan kaolinitic minerals. Steel Res Int. 2006. https://doi.org/10.1002/srin.200606426.
46. GOST 3226-93. Межгосударственный стандарт. Глинны формовочные огнеупорные. Общие технические условия. (Moulded refractory clays. General specifications), The Russian government Federal Agency on Technical Regulating and Metrology; 1994. In: Russian. https://docs.cntd.ru/document/1200024902. Accessed 02 Sept 2022
47. Balabanits DA. Refractory clays of the Toretskoe deposit. Glass Ceram. 2003. https://doi.org/10.1023/A:1025777404762.
48. Lee S, Kim YJ, Moon H-S. Phase transformation sequence from kaolinite to mullite investigated by an energy-filtering transmission electron microscope. J Am Ceram Soc. 1999;82(10):2841–8.
49. Koleda VV, Mikhailyuta ES, Alekseev EV, Tsybul`ko ÉS. Technological particularities of clinker brick production. Glass Ceram. 2009; https://doi.org/10.1007/s10717-009-9129-3
50. Mokrzycki WS, Tatol M. Colour difference Δ*E*—a survey. Mach Graph Vis. 2011;20(4):383–411.

Authors and Affiliations

Milica Vidak Vasić[1] · Lidija Radovanović[2] · Lato Pezo[3] · Zagorka Radojević[1]

[1] Institute for Testing of Materials IMS, Bulevar Vojvode Mišića 43, 11000 Belgrade, Serbia

[2] Innovation Centre of the Faculty of Technology and Metallurgy, University of Belgrade, Karnegijeva 4, 11000 Belgrade, Serbia

[3] Institute of General and Physical Chemistry, University of Belgrade, Studentski Trg 12/V, 11000 Belgrade, Serbia